Article

Not peer-reviewed version

Biogenic Synthesis of Gold Nanoparticles Using *Scabiosa palaestina* Extract: Characterization, Anticancer, and Antioxidant Activities

Heba Hellany , Adnan Badran , Ghosoon Albahri , Nadine Kafrouny , Riham El Kurdi , Marc Maresca * , Digambara Patra , Elias Baydoun *

Posted Date: 5 August 2025

doi: 10.20944/preprints202508.0316.v1

Keywords: *Scabiosa palaestina*; green synthesis; gold nanoparticles; cancer cell lines; antioxidant activity

 doi:10.20944/preprints202508.0316.v1

Article

Biogenic Synthesis of Gold Nanoparticles Using *Scabiosa palaestina* Extract: Characterization, Anticancer, and Antioxidant Activities

Heba Hellany [1], Adnan Badran [2], Ghosoon Albahri [1,3], Nadine Kafrouny [4], Riham El Kurdi [4], Marc Maresca [5,*], Digambara Patra [4] and Elias Baydoun [1,*]

[1] Department of Biology, American University of Beirut, Beirut 1107, Lebanon
[2] Department of Nutrition, University of Petra, Amman 11196, Jordan
[3] Doctoral School of Science and Technology, Research and Analysis Platform in Environmental Sciences (EDST-PRASE), Beirut, Lebanon
[4] Department of Chemistry, American University of Beirut, Beirut 1107, Lebanon
[5] Aix Marseille Univ, CNRS, Centrale Marseille, iSm2, 13013 Marseille, France
* Correspondence: m.maresca@univ-amu.fr (M.M.); eliasbay@aub.edu.lb (E.B.)

Abstract

Gold nanoparticles (AuNPs) are promising materials for the development of novel anticancer agents, and their green synthesis has become essential due to their numerous advantages. This study aimed to synthesize AuNPs using an ethanolic extract of *Scabiosa palaestina*, characterize their physicochemical properties, and evaluate their anticancer properties as well as their antioxidant potential. AuNPs were successfully synthesized and characterized using UV–Visible spectroscopy, scanning electron microscopy (SEM), zeta potential analysis, thermogravimetric analysis (TGA), X-ray diffraction (XRD), and attenuated total reflection Fourier transform infrared spectroscopy (ATR-FTIR). The results indicated that the biosynthesized AuNPs were spherical and well-dispersed, exhibiting an absorption peak at 560 nm and an average size of 9.9 nm. Cytotoxicity assays demonstrated a dose- and time-dependent inhibitory effect on MDA-MB-231, Capan-2, HCT116, and 22Rv1 cancer cell lines, with 22Rv1 and MDA-MB-231 cells showing the most potent responses. At the highest concentration tested (100 µg/ml) after 72 hours, cell viability was reduced to 16.04 ± 1.8% for 22Rv1 and 17.48 ± 8.3% for MDA-MB-231 cells. Additionally, the AuNPs exhibited concentration-dependent antioxidant activity in both DPPH and H2O2 scavenging assays. In summary, the synthesized AuNPs demonstrated multifunctional properties that make them suitable for a wide range of biomedical and biotechnological applications.

Keywords: *Scabiosa palaestina*; green synthesis; gold nanoparticles; cancer cell lines; antioxidant activity

1. Introduction

Nanotechnology is an emerging field with transformative potential across various disciplines. It involves the manipulation of materials at the nanoscale (1–100 nm), where they exhibit unique physical, chemical, and biological properties that differ from bulk materials [1]. It offers promising solutions for complex diseases such as cancer, neurodegenerative disorders, and metabolic syndromes by enabling early detection and targeted treatment [1]. Metallic nanoparticles are among the most versatile types of nanoparticles, given their wide range of applications in chemistry, electronics, medicine, and pharmaceutical sciences [2]. Gold and silver nanoparticles are commonly used in products that come into direct contact with humans, including soaps, detergents, and cosmetics, as well as in various medical and pharmaceutical applications [3].

 doi:10.20944/preprints202508.0316.v1

AuNPs are among the most widely used nanomaterials due to their wide range of appealing properties, particularly the simplicity of surface functionalization. The advantages of AuNPs include straightforward synthesis and characterization, ease of surface modification, low toxicity, tunable surface plasmon resonance, strong biostability, and excellent biocompatibility [4]. Due to their small size, AuNPs can enter cells and interact with various biomolecules without causing harm, making them an ideal choice for drug delivery, cancer therapy, and other therapeutic uses [5]. Cancer nanotechnology, in particular, is gaining significant attention due to its potential to revolutionize cancer diagnosis and therapy [1]. AuNPs have emerged as a powerful tool in cancer research and medicinal chemistry due to their benefits. They are particularly used in cancer drug delivery and bioimaging, where they have been effectively utilized for several years [5, 6].

Nanoparticles can be synthesized using three main approaches: physical, chemical, and biological methods. The synthesis of AuNPs via chemical and physical methods is already well established. However, these approaches often involve the use of toxic chemicals and non-polar solvents, leading to harmful environmental effects and necessitating multiple purification steps, which makes the process costly [7]. In contrast to physical and chemical methods, green synthesis provides several benefits that align with the principles of green chemistry [8]. The green synthesis involves the use of natural compounds derived from plants or microorganisms (such as fungi, bacteria, and algae) to reduce gold ions. This biosynthetic method is regarded as a simple, cost-effective, and environmentally friendly approach, as it typically employs non-toxic solvents like water [2]. While microbial synthesis of gold nanoparticles is eco-friendly, it has notable drawbacks. The process is time-consuming due to long incubation periods, and the intracellular production requires complex purification steps, increasing the cost and effort. Additionally, it often results in nanoparticles with varied sizes and shapes [9]. However, the synthesis of AuNPs using plant-based materials offers several advantages, making it a simple, efficient, and cost-effective approach [9]. This method allows for easy regulation of nanoparticle size and shape by adjusting reaction conditions [9]. Plant extracts, rich in diverse bioactive compounds such as flavonoids, terpenoids, amino acids, aldehydes, and alcohols, serve as both reducing and stabilizing agents due to their high redox potential [2]. For example, Curcumin has been extensively investigated as a reducing and stabilizing agent in the green synthesis of AuNPs [10].

Scabiosa palaestina is a plant species that belongs to the Scabiosa genus, known to be rich in iridoids, flavonoids, and pentacyclic triterpenoids [11]. The current study investigates the biogenic synthesis of AuNPs using the ethanolic extract of *Scabiosa palaestina* for the reduction of $HAuCl_4$. We successfully synthesized AuNPs using *Scabiosa palaestina* extract as both a reducing and stabilizing agent. The synthesized AuNPs were characterized using various analytical techniques to assess their physicochemical properties. In addition, the synthesized AuNPs demonstrated strong antioxidant and anticancer activities.

2. Materials and Methods

2.1. Preparation of Scabiosa palaestina Ethanolic Extract (SPE)

Scabiosa palaestina was acquired from Al Meri in South Lebanon, and it was identified by Mohammad Al Zein, a plant taxonomist at the American University of Beirut's (AUB) Biology Department. The Post Herbarium at AUB has received a voucher specimen with the number GA 2025-3. After washing, the whole plant was air-dried in the dark. The dried plant was ground into fine powder, then suspended in 80% ethanol and shaken constantly in the dark for 72 hours. The solution was filtered, condensed with a rotary vacuum evaporator, and then freeze dried. Gold nanoparticles were synthesized using the resulting powder.

2.2. Green Synthesis of Gold Nanoparticles Using SPE

The green synthesis of AuNPs **(Scheme 1)** was based on previous work [12] with some modifications, where the ratio of materials used in the synthesis was doubled compared to the

 doi:10.20944/preprints202508.0316.v1

original study (4:1 instead of 2:1). *Scabiosa palaestina* ethanolic extract and gold (III) chloride trihydrate ($HAuCl_4 \cdot 3H_2O$) (Acros Organic) were combined in a 4:1 ratio and dissolved in 20 mL of double-distilled water. The mixture was heated at 70–80 °C and sonicated for 30 minutes, during which a color change from green to dark purple indicated nanoparticle formation. The resulting solution was centrifuged at 15,000 rpm for 15 minutes. The pellet containing AuNPs was resuspended in double-distilled water, lyophilized, and the resulting powder was stored at 4 °C for subsequent use.

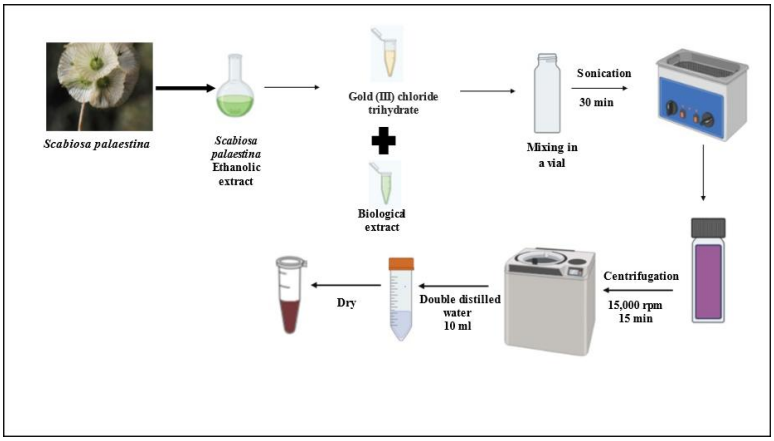

Scheme 1. Green synthesis of AuNPs using *Scabiosa palaestina* ethanolic extract.

2.3. Characterization of AuNPs

A key indicator of successful green synthesis of AuNPs with plant ethanolic extract is the observed color change of the solution. The optical absorption corresponding to the purple color intensity of the synthesized AuNPs was measured at room temperature using a UV–Visible spectrophotometer (JASCO V-570 UV–Vis–NIR) in scanning mode, with the wavelength range of 450 to 800 nm to determine the peak absorbance [7], with a resolution of 1 nm, as described by Jyoti et al. [13].

Scanning Electron Microscopy (SEM) using a MIRA3 LMU instrument was employed to examine the shape of AuNPs, which were diluted, air-dried, and mounted on carbon-coated aluminum stub. Simultaneously, energy-dispersive X-ray spectroscopy (EDX) using an OXFORD detector was employed to confirm the elemental composition of the AuNPs.

The zeta (ζ) potential of the synthesized AuNPs and SPE, as well as the size distribution of AuNPs, were evaluated using the dynamic light scattering (DLS) technique (Brookhaven Instruments Corps), equipped with a 658 nm laser source and a PMT detector (HAMAMATSU, HC120-30). The 90Plus Particle Sizing Software (Version 5.23) was used for analysis, with the dust parameter set to 40.

The thermal stability of SPE and AuNPs was evaluated using thermogravimetric analysis (TGA) with a Netzsch TGA 209 instrument under a nitrogen atmosphere. The analysis was performed on 5 mg samples placed in aluminum oxide (Al_2O_3) crucibles, over a temperature range of 30 to 900 °C, with a heating rate of 15 K/min.

The crystalline structure of the AuNPs was analyzed using X-ray diffraction (XRD) with a Bruker D8 Advance diffractometer. The samples were collected as fine powder and mounted on a zero-background holder. Scanning was performed in coupled 2θ/θ mode over a 2θ range of 30° to 80°, with a step size of 0.02°

The presence of functional groups corresponding to specific molecules or metabolites in the plant aqueous extract and their role were assessed using Fourier-transform infrared spectroscopy with attenuated total reflectance (FTIR-ATR) [14]. Spectra were recorded with a Bruker Tensor 27 FT-IR instrument equipped with a diamond ATR module.

2.4. Cell Culture

 doi:10.20944/preprints202508.0316.v1

Human breast cancer MDA-MB-231 cells (ATCC, Manassas, VA, USA) and Capan-2 pancreatic cancer cells (CLS, Eppelheim, Germany) were cultured in high-glucose DMEM supplemented with 10% fetal bovine serum (FBS) and 1% penicillin/streptomycin (both from Sigma-Aldrich, St. Louis, MO, USA; antibiotics from Lonza, Switzerland).

Human colorectal cancer HCT116 cells and prostate cancer 22RV1 cells (both from ATCC, Manassas, VA, USA) were maintained in RPMI-1640 medium (Sigma-Aldrich) supplemented with 10% FBS, 1% penicillin/streptomycin, and 1% sodium pyruvate.

All cell lines were incubated at 37 °C in a humidified atmosphere containing 5% CO_2.

2.5. MTT Cell Viability Assay

Cell viability was assessed using the MTT reduction assay (3-(4,5-dimethylthiazol-2-yl)-2,5-diphenyltetrazolium bromide; Sigma-Aldrich, St. Louis, MO, USA). Cells were seeded in 96-well tissue culture plates at a density of 5×10^3 cells per well and incubated for 24 hours to reach 30–40% confluency. Following incubation, the culture medium was replaced with fresh medium containing varying concentrations of AuNPs (5, 10, 25, 50, 75 and 100 µg/ml), and cells were further incubated for 24, 48, and 72 hours. Following the incubation period, 20 µl of fresh MTT solution was added to each well. The plates were then incubated in the dark for an additional 2 hours at 37 °C. Then, the MTT solution was discarded, and 200 µl of 10% DMSO was added to dissolve the resulting formazan crystals.

Absorbance was measured at 595 nm using a microplate reader. Each condition was tested in triplicate, and experiments were independently repeated three times. Cell proliferation was expressed as the percentage of viable cells relative to vehicle-treated controls (DMSO), which were considered 100% viable. Cell viability was calculated using the following formula [7]:

$$\text{Cell viability (\%)} = \frac{\text{Absorbance of treated samples}}{\text{Absorbance of control}} \times 100$$

2.6. Microscopic Analysis of Apoptotic Morphological Changes

MDA-MB-231 cells were cultured in 6-well plates with or without the specified concentrations of the Au-NPs. After 24 hours, morphological features characteristic of apoptosis were examined using an inverted phase-contrast microscope at magnifications of ×10, ×20, and ×40.

To assess nuclear morphological changes, cells were stained with 4′,6-diamidino-2-phenylindole (DAPI) (Cell Signaling #4083). For this, cells were seeded in 12-well plates and treated with the indicated concentrations of Au-NPs for 24 hours, followed by fixation with 4% formaldehyde, DAPI staining, and observation under a fluorescence microscope.

2.7. Antioxidant Activity

2.7.1. DPPH Free Radical Scavenging Assay

The antioxidant activity of *Scabiosa palaestina*-synthesized AuNPs was evaluated using the standard DPPH (2,2-diphenyl-1-picrylhydrazyl) free radical scavenging assay, with ascorbic acid serving as the reference compound. Various concentrations of the synthesized AuNPs (5, 10, 25, 50, 75, and 100 µg/ml) were prepared in DMSO. Briefly, 1 mL of 0.1 mM DPPH solution (prepared in methanol) was added to 1 mL of each AuNPs or ascorbic acid solution. A blank control was also prepared by replacing the AuNPs or ascorbic acid with 1 mL of DMSO. All mixtures were incubated in the dark for 30 minutes at room temperature. The absorbance of each solution was then measured at 517 nm, and the percentage of radical scavenging activity was calculated using the appropriate formula [15]:

$$\text{Scavenging inhibition (\%)} = \frac{\text{Absorbance of control} - \text{absorbance of tested sample}}{\text{Absorbance of control}} \times 100$$

The experiment was performed in triplicate, and the results are expressed as mean ± SEM.

 doi:10.20944/preprints202508.0316.v1

2.7.2. Hydrogen Peroxide Radical Scavenging (H_2O_2) Assay

The antioxidant activity of AuNPs was also assessed based on their ability to scavenge hydrogen peroxide. A 40 mM hydrogen peroxide solution was prepared in 1 M phosphate buffer (pH 7.4), and various concentrations of synthesized AuNPs, prepared in DMSO, were added to the hydrogen peroxide solution and incubated for 10 minutes. After incubation, 2 ml of dichromate-acetic acid reagent was added to each reaction mixture. A blank containing only phosphate buffer without hydrogen peroxide was used as a reference, while a reaction mixture without AuNPs served as the control [16]. The absorbance was measured at 570 nm, and the percentage of hydrogen peroxide scavenging was calculated as follows:

$$\text{Scavenging inhibition (\%)} = \frac{\text{Absorbance of control} - \text{absorbance of tested sample}}{\text{Absorbance of control}} \times 100$$

The experiment was performed in triplicate, and the results are expressed as mean ± SEM.

2.8. Statistical Analysis

Statistical analysis was performed using two-way ANOVA followed by Tukey–Kramer post hoc test. Results are expressed as mean ± SEM, and $p < 0.05$ was considered significant.

3. Results

3.1. Green Synthesis of Gold Nanoparticles Using SPE

The successful synthesis of AuNPs was first indicated by a color change in the reaction mixture, which shifted from dark yellowish green to purple. The immediate appearance of a purple color upon adding the *Scabiosa palaestina* confirmed the formation of AuNPs (Figure 1).

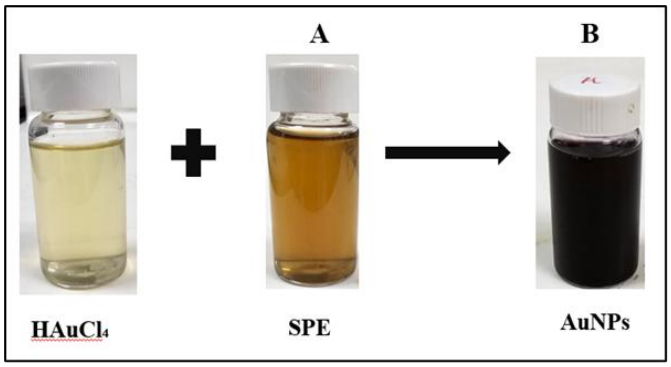

Figure 1. Visual confirmation of AuNPs synthesis based on color change: **(A)** Before the addition of $HAuCl_4 \cdot 3H_2O$ to the *Scabiosa palaestina* ethanolic extract (SPE), and **(B)** following the addition of $HAuCl_4 \cdot 3H_2O$ to SPE.

3.2. Characterization of Biosynthesized AuNPs

3.2.1. UV- Vis Spectrometry

The intensity of the purple color, which was considered the first sign of green AuNPs synthesis, was analyzed using UV- Vis spectroscopy to identify the surface plasmon resonance (SPR) peak. SPR is a unique characteristic of noble metal nanoparticles, generating strong electromagnetic fields at their surfaces, which enhances radiative properties like light scattering and absorption [14]. As shown in Figure 2, the colloidal solution exhibited an SPR peak at 560 nm, indicative of the successful reduction of Au^{3+} ions and the formation of gold nanoparticles. The observed peak at 560 nm, slightly red-shifted relative to the typical 520 nm peak for small spherical AuNPs, suggests the formation of larger-sized particles and/or a degree of aggregation. This shift may be attributed to the influence of

 doi:10.20944/preprints202508.0316.v1

phytochemicals in *Scabiosa palaestina* extract, which act as both reducing and stabilizing agents during nanoparticle synthesis.

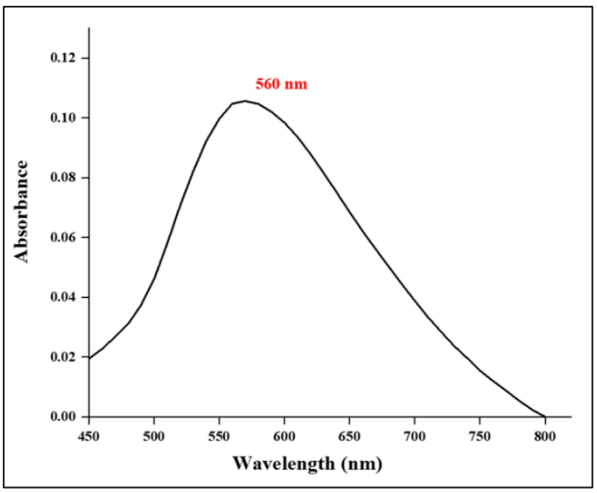

Figure 2. UV- Vis spectra of AuNPs formed through *S. palaestina* ethanolic extract.

3.2.2. Morphological and Elemental Analysis – SEM and EDX

The morphology and size of the synthesized AuNPs were examined using SEM (Figure 3). The analysis revealed the production of spherical Au NPs with a small size of less than 50 nm. The analysis also showed a certain level of nanoparticle aggregation.

According to EDX analysis (Figure 4), a strong peak around 2.2 keV confirmed the presence of gold in the sample, and gold constituted about 20% of the sample by mass. These results indicate that gold was successfully incorporated into the composition of the synthesized nanoparticles. The presence of additional peaks (Carbon, Oxygen) is attributed to phytochemicals present in the *Scabiosa palaestina* ethanolic extract.

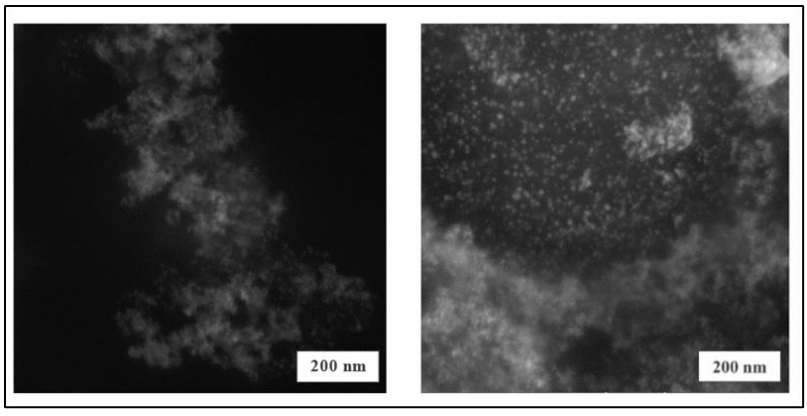

Figure 3. SEM micrograph showing the morphology of synthesized AuNPs with a scale bar of 200 nm.

 doi:10.20944/preprints202508.0316.v1

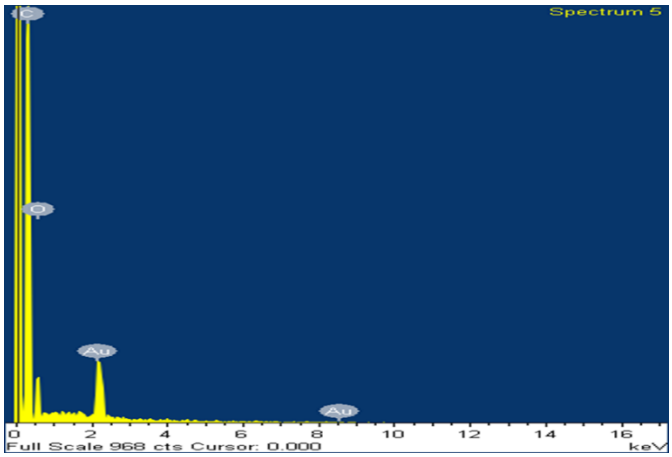

Figure 4. The elemental composition of synthesized AuNPs by EDX analysis.

3.2.3. Particle Size and Zeta Potential

DLS technique was used to assess the average particle size and size distribution of synthesized AuNPs. As illustrated in Figure 5, the nanoparticles showed an average size of 9.9±1.3 nm based on the size distribution graph, with a polydispersity index (PDI) of 0.172.

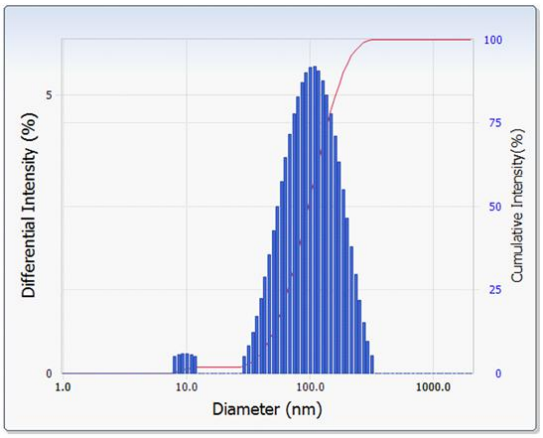

Figure 5. Size distribution of Scabiosa palaestina synthesized AuNPs via DLS.

Moreover, Zeta potential measurements were conducted to assess the surface charge and colloidal stability of AuNPs synthesized from *Scabiosa palaestina* ethanolic extract, compared to the extract. Negative zeta potential values were observed for both samples, measured at -17.6 mV for the AuNPs and -9.9 mV for the plant ethanolic extract (Figure 6). The more negative zeta potential of the nanoparticles indicates enhanced electrostatic repulsion between particles, contributing to greater colloidal stability. This increase in surface charge is attributed to the adsorption of negatively charged phytochemicals from the extract onto the nanoparticle surface during synthesis, suggesting successful capping and stabilization of the nanoparticles by bioactive constituents.

 doi:10.20944/preprints202508.0316.v1

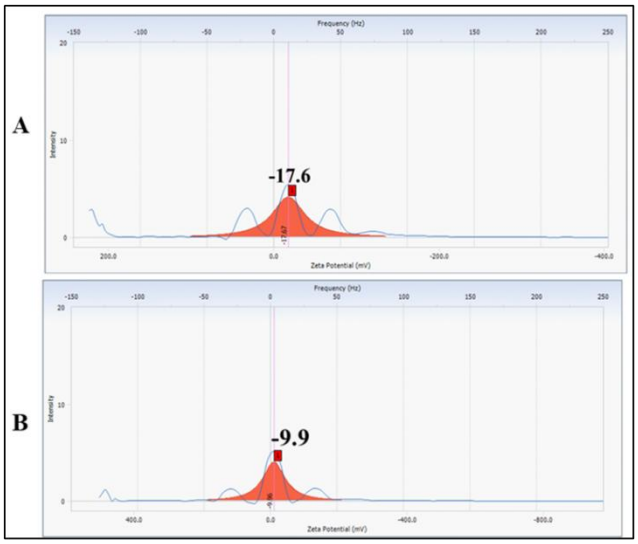

Figure 6. Zeta potential values of **(A)** AuNPs and **(B)** SPE.

3.2.4. TGA Analysis

The thermal stability of the biosynthesized AuNPs and *Scabiosa palaestina* ethanolic extract was further verified using TGA. As shown in Figure 7, the plant extract (red curve) displayed initial thermal stability up to approximately 120 °C, after which a rapid weight loss occurred, indicating the evaporation of moisture and low-molecular-weight volatiles. Significant degradation was observed between 150 °C and 450 °C, with the extract undergoing a total mass loss of approximately 78% and stabilizing with ~22% residual weight at around 600 °C. In contrast, the AuNPs (black curve) demonstrated improved thermal resistance, remaining stable up to 150 °C and exhibiting a more gradual decomposition profile from 200 °C to 700 °C. At the end of the thermal scan (~800 °C), the AuNPs retained approximately 45% of their original weight, indicating a total mass loss of about 55%. This enhanced thermal stability of the AuNPs suggests successful surface capping of the nanoparticles by phytochemicals from the *Scabiosa palaestina* extract. The interaction between bioactive compounds and the gold core likely results in a more stable organic–inorganic hybrid structure, which slows down thermal degradation.

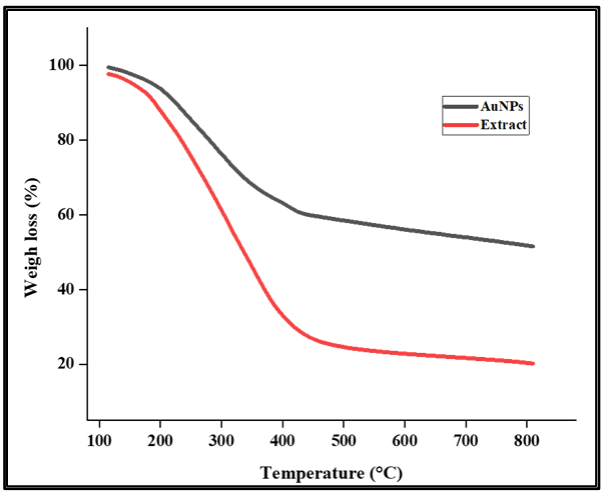

Figure 7. TGA analysis of SPE as well as the biosynthesized AuNPs.

3.2.5. Crystallinity Characterization

 doi:10.20944/preprints202508.0316.v1

XRD analysis was performed to verify the crystalline structure of the gold nanoparticles synthesized using SPE extract. The XRD patterns demonstrated four prominent diffraction peaks at 2θ values of 38.03°, 46.18°, 63.43°, and 77.18° sets of lattice planes (Figure 8). The observed planes were assigned to the (111), (200), (220), and (311) facets of the synthesized gold nanoparticles. These XRD patterns confirm the formation of a face-centered cubic (FCC) crystalline structure, according to the Joint Committee on Powder Diffraction Standards (JCPDS Card Number 04-0783) [17]. The strong intensity of the (111) peak further suggests a preferential orientation along this plane, which is commonly observed in biosynthesized gold nanoparticles. Overall, the XRD results confirm the successful formation of crystalline AuNPs with a typical FCC structure.

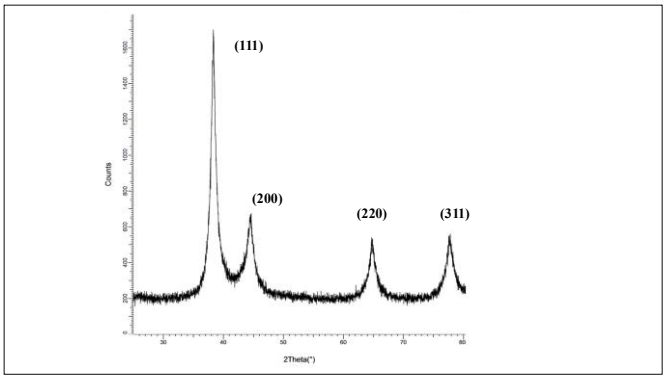

Figure 8. XRD pattern of AuNPs obtained by using SPE.

3.2.6. FTIR Analysis

FTIR analysis was conducted to determine the functional groups in the plant extract and the biosynthesized AuNPs. As shown in Figure 9, ten distinctive peaks were observed in the *Scabiosa palaestina* ethanolic extract at wavenumbers 3336, 2971, 2919, 1609, 1380, 1252, 1154, 1070, 818, and 527 cm^{-1}. These were attributed to hydrogen-bonded O–H and N–H stretching (3336 cm^{-1}), C–H stretching of aliphatic groups (2971, 2919 cm^{-1}), C=O stretching from carbonyl-containing compounds (1609 cm^{-1}), and various C–N, C–O, and aromatic ring vibrations in the fingerprint region (1380–527 cm^{-1}), suggesting the presence of polyphenols, amines, and other bioactive molecules. In comparison, the spectrum of AuNPs exhibited peaks at 3930, 2916, 2853, 1726, 1613, 1466, 1380, 1264, 1179, 1050, and 430 cm^{-1}. Notable differences included the appearance of an additional peak at 1726 cm^{-1}, likely corresponding to a newly formed or shifted carbonyl group, and the disappearance of the broad hydrogen-bonded O–H/N–H stretching band at 3336 cm^{-1}, indicating the involvement of these groups in the reduction and stabilization processes. Additionally, several peaks exhibited slight shifts and intensity reductions, particularly in the 1600–1000 cm^{-1} region. These changes were accompanied by a marked decrease in transmittance variation, as the Y-axis range narrowed from 100–95% in the extract to 99.9–99.5% in the AuNP spectrum, reflecting a reduction in free functional groups due to their participation in gold ion reduction and nanoparticle capping.

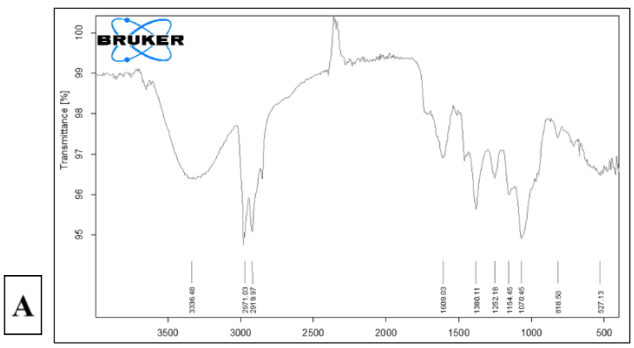

A

 doi:10.20944/preprints202508.0316.v1

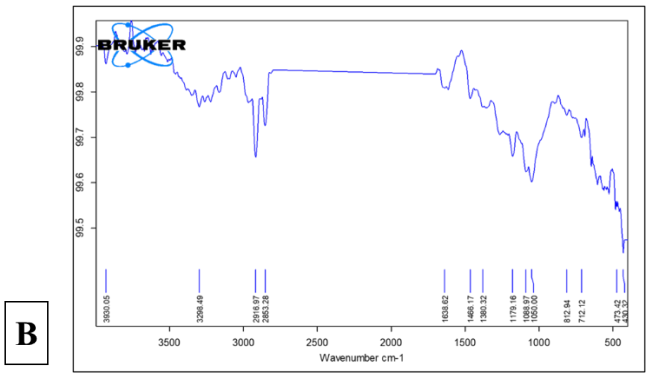

Figure 9. ATR-FTIR spectrum of **(A)** SPE and **(B)** AuNPs.

3.3. Anticancer Activity of Biosynthesized AuNPs

Following the successful synthesis and characterization of AuNPs using *Scabiosa palaestina* ethanolic extract, their anticancer activity was investigated against four human cancer cell lines: pancreatic (Capan-2), prostate (22RV1), colorectal (HCT116), and breast (MDA-MB-231), using the MTT assay at various concentrations (0, 10, 25, 50, 75, and 100 µg/ml) and exposure times (24 h, 48 h, 72 h). A concentration- and time-dependent reduction in cell viability was observed across all tested cell lines (Figure 10). Among the tested cell lines, 22Rv1 and MDA-MB-231 cells exhibited a more pronounced cytotoxic response at higher AuNP concentrations, particularly after 72 hours of treatment. At 72 hours, cell viability for 22Rv1 cells decreased to 23.51 ± 0.5%, 17.37 ± 0.8%, and 16.04 ± 1.8% at concentrations of 50, 75, and 100 µg/mL, respectively. Similarly, MDA cell viability was reduced to 27.87 ± 2.4%, 25.30 ± 2.8%, and 17.48 ± 8.3% at the same concentrations. The half-maximal inhibitory concentration (IC_{50}) values for all cell lines were calculated and are presented in Table 1.

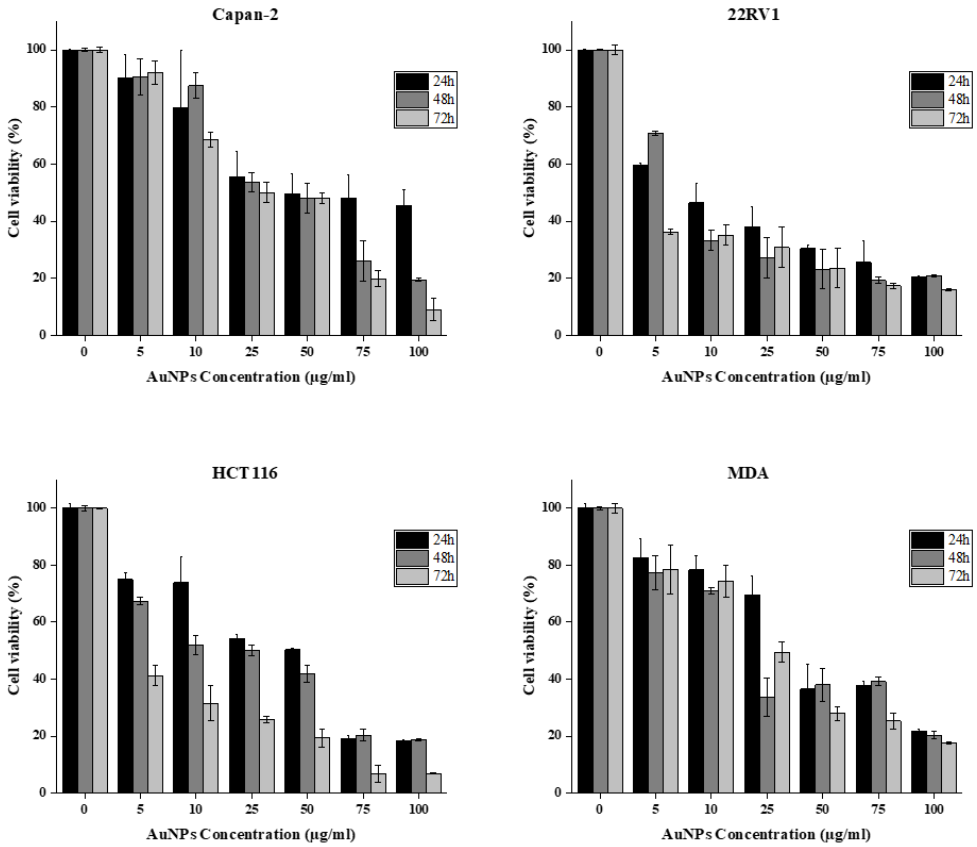

 doi:10.20944/preprints202508.0316.v1

Figure 10. Cytotoxicity assay of synthesized AuNPs on different cancer cell lines: Breast (MDA-MB-231), pancreatic (Capan-2), prostate (22Rv1), and colon (HCT116). Results are presented as the mean ± SEM from three independent experiments (n = 3) and expressed as a percentage relative to the corresponding control group. *p*-values were calculated, and $p < 0.05$ was considered statistically significant.

Table 1. IC_{50} values for all cell lines after 72h of treatment with SPE-synthesized AuNPs.

Cell line	IC_{50} (µg/ml)
Capan-2	4.0
22RV1	2.3
HCT116	2.2
MDA-MB-231	3.3

To better understand how AuNPs biosynthesized by SPE reduce cancer cell viability, we examined apoptosis induction in MDA-MB-231 breast cancer cells treated with two concentrations of these nanoparticles (25 and 50 µg/ml). Cell morphology was observed after 24 hours of AuNPs exposure using an inverted phase-contrast microscope. Image analysis revealed a concentration-dependent decline in the total number of cells within the microscopic fields. Apoptosis was further confirmed by identifying echinoid spikes and membrane blebbing **(Fig. 11A).** Additionally, examination of DAPI-stained, AuNP-treated cells demonstrated chromatin fragmentation, nuclear condensation, and clustering of apoptotic bodies **(Fig. 11B)**. Collectively, these findings provide strong evidence that the anticancer effects of AuNPs involve the activation of apoptotic pathways.

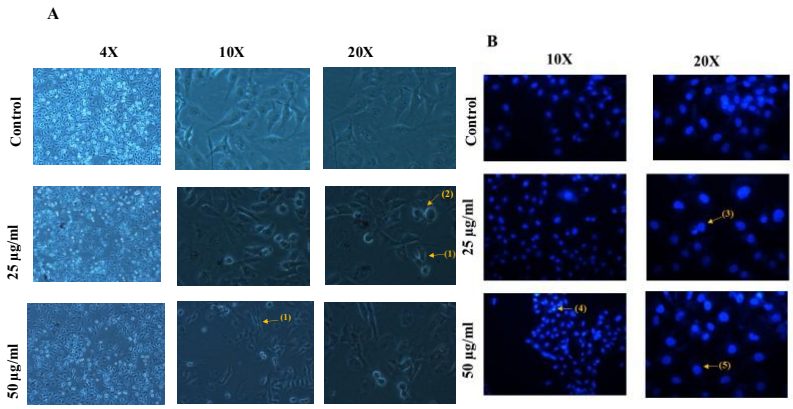

Figure 11. *Scabiosa palaestina* synthesized AuNPs induce apoptosis in MDA-MB-231 cells. **(A):** MDA-MB-231 cells were exposed to various concentrations of AuNPs for 24 hours, with or without treatment. Morphological alterations were examined using light microscopy. Arrows highlight: **(1)** echinoid spikes, **(2)** membrane blebbing. **(B):** Similarly, MDA-MB-231 cells were treated with different concentrations of AuNPs or left untreated for 24 hours, followed by staining with DAPI to visualize nuclear structures. Fluorescence microscopy was used to detect nuclear morphological changes, with arrows indicating**: (3)** apoptotic bodies, **(4)** nuclear condensation, **(5)** chromatin lysis.

3.4. Antioxidant Activity

3.4.1. DPPH Assay

The antioxidant activity of synthesized AuNPs was studied first using the DPPH assay, with ascorbic acid serving as the positive control. DPPH, a lipophilic and stable free radical, easily accepts a hydrogen electron from antioxidant compounds, which causes a color change from purple to yellow that can be measured at 517 nm [18]. The biosynthesized AuNPs exhibited excellent antioxidant activity, showing significantly greater free radical inhibition than the standard ascorbic acid ($p<0.05$).

 doi:10.20944/preprints202508.0316.v1

Additionally, the free radical-scavenging ability of the biosynthesized AuNPs exhibited a dose-dependent pattern, with antioxidant activity increasing as the concentration rises. As shown in Figure 12, at a concentration of 100 µg/ml, AuNPs exhibited a maximum inhibition percentage of 95%, compared to the standard antioxidant ascorbic acid, which showed 90% inhibition.

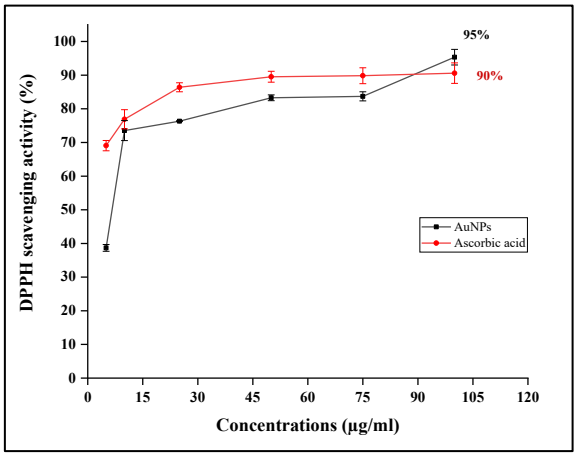

Figure 12. Antioxidant scavenging potential of synthesized AuNPs using DPPH assay. Results are expressed in terms of mean ± SEM (n = 3).

3.4.2. H_2O_2 assay

Another important antioxidant assay conducted was the hydrogen peroxide assay. H_2O_2 is not a free radical itself, but can cause significant harm in biological systems by promoting the formation of reactive radicals. When present in high concentrations, H_2O_2 interacts with transition metals such as iron or copper through the Fenton reaction, generating highly reactive hydroxyl radicals (HO·) [19, 20]. The synthesized AuNPs exhibited strong H_2O_2 scavenging activity. Figure 13 illustrates the hydrogen peroxide scavenging activity of AuNPs synthesized using *S. palaestina* ethanolic extract. The scavenging activity increased progressively with higher concentrations of biosynthesized AuNPs (dose-dependent manner). The H_2O_2 scavenging activity of AuNPs increased from 56% at the lowest concentration (5 µg/mL) to 83% at the highest concentration (100 µg/mL). Notably, the inhibition observed at the highest concentration surpassed that of the positive control, which showed 78% scavenging activity.

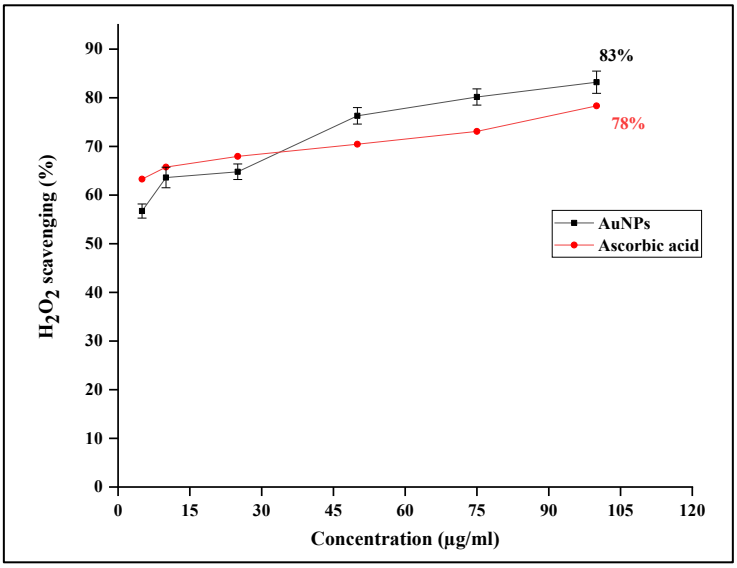

Figure 13. Antioxidant scavenging potential of synthesized AuNPs using Hydrogen Peroxide assay. Results are expressed in terms of mean ± SEM (n = 3).

 doi:10.20944/preprints202508.0316.v1

4. Discussion

In the current study, the ethanolic extract of *Scabiosa palaestina* was utilized for the green synthesis of AuNPs. According to earlier studies, *Scabiosa palaestina* is a rich source of various metabolites, including flavonoids [21], terpenoids [11, 22], lipids, and organic acids [11, 22]. These metabolites act as biocatalysts and reducing agents, often in synergy with reductase enzymes, to convert metal ions and their oxides into nanoscale structures [7]. During this green synthesis process, these bioactive compounds not only induce a color change in the solution but also facilitate the reduction of $HAuCl_4 \cdot 3H_2O$ to gold nanoparticles, followed by capping and stabilization through proteins and other extracted phytochemicals [23]. In addition, the presence of starch and glucose in the plant extracts acts as a reducing and stabilizing agent in the synthesis of AuNPs [24]. The successful synthesis of AuNPs was initially validated by the immediate appearance of a purple color upon the addition of $HAuCl_4 \cdot 3H_2O$ to *Scabiosa palaestina* ethanolic extract. The development of purple color following the reaction between $HAuCl_4$ solution and the ethanolic extract of *Pelargonium Graveolen* was reported [24], and similar results were reported for *Ricinus communis* [25] and *Pistacia integerrima* [26].

UV-Vis spectroscopy is a highly effective and commonly employed approach for the characterization of nanoparticle structure due to its ability to detect SPR phenomena [25]. Nanoparticles that are composed of noble metals like gold and silver exhibit stronger SPR bands compared to other metals. The intensity and absorption peak of SPR are influenced by various factors, including particle size, shape, and structural properties [6]. The determination of nanoparticle size is essential for their application, and the localized surface plasmon resonance (LSPR) serves as a valuable indicator for size estimation. This phenomenon results from the collective oscillation of conduction band electrons in response to electromagnetic radiation [27]. Gold nanoparticles exhibit LSPR absorption peaks in the visible spectrum, generally between 500 and 600 nm, where the absorption of AuNPs increases with their size [12]. In addition, the alteration of the shape of AuNPs from spherical to rod-shaped AuNPs causes a red shift in the LSPR peak, moving it from the visible region into the near-infrared (NIR) range [28]. In the current study, the absorbance peak at 560 nm indicates the successful synthesis of spherical AuNPs with a relatively small diameter. This result is in accordance with previous studies on biosynthesized AuNPs exhibiting a spherical shape and small diameter [7, 25, 29–31].

SEM analysis was used to determine the shape, size, and aggregation of AuNPs synthesized. The bioactive compounds present in the ethanolic extract of *Scabiosa palaestina* facilitated the synthesis of spherical, well-dispersed, and small AuNPs with a size of less than 50 nm. These results are consistent with previous studies, where the size of AuNPs synthesized from different plant extracts similarly ranged from 5–53 nm [7], 6.06–17.36 nm [32], 15 nm [33], and 40–85 nm [34], indicating a consistency in nanoparticle dimensions. However, the differences in average particle sizes may be due to the distinct metabolites present in each plant extract, which act as reducing, capping, and stabilizing agents during AuNPs synthesis [7]. EDX analysis confirmed the presence of gold in the composition of the biosynthesized nanoparticles. In addition, the presence of Carbon and Oxygen peaks in the EDX spectrum is likely due to the phytochemicals from *Scabiosa palaestina* extract, which served as reducing and capping agents [30, 32]. This indicates that the biological synthesis approach produces AuNPs coated with organic compounds, contributing to improved stability and biocompatibility of the synthesized AuNPs. These organic compounds not only stabilize the nanoparticles but also introduce functional groups, such as phenolics, that are useful for further bioconjugation [35].

According to DLS analysis, the average size of the biosynthesized AuNPs was found to be 9.9 nm. The particle size of our biosynthesized AuNPs, as determined by DLS analysis, was in agreement with SEM results, both indicating that the nanoparticles in our samples were smaller than 50 nm. In a study conducted by Kalantri and Turner et al., AuNPs synthesized through ginger extract displayed an average particle size of 16.83 nm [35]. A similar result was obtained where DLS analysis indicates that the AuNPs synthesized using *Sargassum swartzii* extract have sizes ranging between 14 and 70

 doi:10.20944/preprints202508.0316.v1

nm [36]. Furthermore, PDI provides insights into the uniformity of particle size distribution: PDI values <0.4 indicate a uniform and homogenous suspension, whereas PDI values > 1 suggest a heterogeneous distribution [37]. In our study, the PDI calculated from DLS analysis was found to be 0.172, indicating the formation of uniform AuNPs with a homogenous size distribution. This favorable size distribution enhances both stability and functionality of AuNPs, which are essential for biomedical applications [35].

Zeta potential, also known as electrokinetic potential, refers to the electrical potential that enables particle movement in a colloidal solution under an applied electric field. It is considered a reliable indicator of the stability of biosynthesized nanoparticles [7]. According to established guidelines, zeta potential values within ±0–10 mV indicate highly unstable particles, ±10–20 mV suggest relative stability, ±20–30 mV reflect moderate stability, and values greater than ±30 mV correspond to highly stable nanoparticles [38]. In our study, the zeta potential of the AuNPs was measured at -17.6 mV, confirming their colloidal stability. Regarding the *Scabiosa palaestina* extract, its zeta potential (-9.9 mV) was lower in magnitude than that of the synthesized AuNPs. These findings align with those obtained by Xin Lee et al. [39], where the plant extract exhibited a zeta potential of -14.68mV, while the AuNPs synthesized from it showed a more negative zeta potential of -20.82mV. The zeta potential of AuNPs is typically more negative (i.e., has a higher absolute value) compared to the original plant extract. This increase in negative surface charge is due to the adsorption of negatively charged phytoconstituents and capping agents from the extract onto the nanoparticle surface during synthesis [40].

The TGA analysis graph of the biosynthesized AuNPs exhibited a two-stage weight loss process. The first phase, which occurred between 100°C and 200°C, corresponds to the loss of water adsorbed by the capping agents from the extract [2, 12, 17]. The second phase, which was more significant, between 200°C and 500°C, is attributed to the thermal decomposition and combustion of the thin organic layer capping the nanoparticles. This layer primarily originates from the phytochemicals present in the SPE, which act as reducing and stabilizing agents during the green synthesis process [41, 42]. Additionally, it is assumed that the degradation of thermally stable aromatic compounds and biogenic salts takes place after 350-400 °C [2, 41]. These results suggest that the SPE compounds provide a protective layer on the surface of the synthesized AuNPs.

The crystalline structure of the plant-mediated AuNPs was analyzed using XRD, and the diffraction peaks observed in the XRD pattern correspond to a face-centered cubic (FCC) crystal lattice. Furthermore, the absence of any additional peaks confirms the high purity of the synthesized AuNPs. Our results are in agreement with previously reported data on the green synthesis of AuNPs using plant extracts [17, 25, 32, 41].

FTIR-ATR analysis of SPE and synthesized AuNPs revealed both similarities and differences, reflecting the involvement of specific functional groups in the synthesis of AuNPs. Various functional groups found in plant extracts —such as amines, carbohydrates, proteins, and amino acids—can participate in the reduction, capping, and stabilization of the synthesized AuNPs [7]. Several peaks remained unchanged between the two spectra, indicating functional groups not directly involved in the synthesis. Notably, the peak at 1380 cm^{-1}, attributed to C–H stretching vibrations, was present in both spectra, suggesting that this functional group was not directly involved in the synthesis process [7]. In contrast, distinct changes were observed in other regions of the spectra, highlighting the interaction of various biomolecules during nanoparticle synthesis. The FTIR spectra of SPE showed a prominent peak at 3,395 cm^{-1} present in the SPE spectrum, which is attributed to the O-H stretching of phenolic compounds and/or N-H (amine) stretching vibration of proteins, disappeared in the spectra of AuNPs, suggesting that hydroxyl and/or amine groups participated in the reduction of Au^{3+} to Au^{0} [30, 35]. Peaks in the 1600-1613 cm^{-1} range, attributed to C=O stretching in carbonyl groups, also shifted, indicating their possible role in metal ion coordination [25]. Additionally, a little shifting was observed from 1252, 1154, 1070 cm^{-1} in the extract, which moved to 1264, 1179, 1050 cm^{-1} in the AuNPs. These bands correspond to C–O/C–N stretches, suggesting the role of flavonoids, phenolic acids, and proteins as capping and stabilizing agents [12].

 doi:10.20944/preprints202508.0316.v1

The advancements in therapeutic nanotechnology involving gold nanoparticles, particularly for cancer diagnosis and treatment, necessitate extensive toxicological studies to establish safe and effective dosing for patients [43]. In this study, an MTT assay was conducted to assess the nanotoxicity of AuNPs synthesized using *Scabiosa palaestina* on various cancerous cell lines. Our results showed that AuNPs exhibited strong cytotoxic effects on all tested cancer cell lines in a dose- and time-dependent manner. These results are consistent with previous findings showing that the AuNPs synthesized from plant extracts exhibited potent anticancer activity against various cell lines [7, 14, 25, 30, 44]. The size of AuNPs significantly influences their cytotoxicity, with smaller particles (10–20 nm) showing increased cellular uptake and, consequently, greater cytotoxic effects [44]. This observation aligns with our results, as the synthesized AuNPs measured less than 20 nm in size and exhibited strong cytotoxic activity. In addition, IC_{50} values were calculated and ranged from 2.29 to 4 μg/ml. As stated by the U.S. National Cancer Institute, extracts exhibiting IC_{50} values ≤ 30 μg/ml are considered to possess a strong cytotoxic activity [2]. This indicates that our synthesized AuNPs exhibited potent cytotoxic activity, as their IC_{50} values fall well below the U.S. National Cancer Institute's threshold, confirming their potential as effective anticancer agents. Nanoparticles have emerged as promising agents in cancer therapy due to their unique physicochemical properties and cellular interactions. Their enhanced cytotoxic effects on cancer cells are largely attributed to their efficient penetration through cellular membranes and strong affinity for biological macromolecules [15]. One key mechanism underlying this cytotoxicity is the generation of reactive oxygen species (ROS), which can cause significant cellular damage and trigger apoptosis [30]. ROS are known to disrupt mitochondrial membrane integrity, thereby activating apoptotic signaling pathways that ultimately lead to cell death or notable changes in cell morphology [7].

The synthesized AuNPs in this study demonstrated strong antioxidant activity as evidenced by the DPPH assay, consistent with findings reported in other studies involving plant-mediated synthesis of gold nanoparticles. For instance, AuNPs synthesized using *Couroupita guianensis* exhibited approximately 70.6% inhibition at their maximum tested concentration [18]. Similarly, gold nanoparticles produced from *Nerium oleander* extracts showed a comparable antioxidant effect, with around 70% inhibition [3]. Notably, AuNPs derived from *Zingiber officinale* demonstrated even higher activity, reaching up to 87% inhibition [7]. Meanwhile, AuNPs synthesized from *Equisetum diffusum* exhibited slightly lower antioxidant potential, with an inhibition rate of 68% [45]. The antioxidant activity of biologically synthesized AuNPs may result from their capacity to donate a hydrogen atom or electron at the atomic level to the DPPH• free radical, thereby reducing it to its stable form, DPPH-H [46].

Hydroxyl radicals generated by the reaction of H_2O_2 with transition metals initiate damaging processes, notably lipid peroxidation in cell membranes, which ultimately lead to cellular damage and impaired function [20]. Therefore, assessing the antioxidant activity of AuNPs using the H_2O_2 scavenging assay is important. The synthesized AuNPs demonstrated excellent hydrogen peroxide (H_2O_2) scavenging activity, consistent with findings reported in other studies involving AuNPs synthesized from various plant sources. For instance, AuNPs derived from the seaweed *Sargassum longifolium* exhibited a maximum H_2O_2 inhibition of approximately 80% [47], while AuNPs synthesized using *Elettaria cardamomum* showed a maximum inhibition of around 38% [48]. The surface reactivity and large surface area-to-volume ratio of nanoparticles can significantly impact their interaction with free radicals, enhancing their scavenging ability and leading to increased antioxidant activity [49]. The antioxidant activity of the nanoparticles is enhanced by plant-derived secondary metabolites—such as sesquiterpenes, phenolics, and flavonoids—which are involved also in both the synthesis and capping of the AuNPs [7].

In this study, the synthesized AuNPs were found to exert cytotoxic effects against various cell lines, primarily through the induction of oxidative stress. However, they also exhibited remarkably high antioxidant activity. This apparent conflict can be attributed to the complex role of mitochondria in the production of free radicals and the multifaceted nature of oxidative stress induced by nanoparticles [50, 51]. The generation of oxidative stress by AuNPs is influenced by various factors,

 doi:10.20944/preprints202508.0316.v1

including non-cellular parameters such as the presence of metal ions, particle size and surface area, concentration, and the synthesis method employed. Additionally, cellular factors like the interaction between nanoparticles and cellular components further modulate their biological effects [50, 51]. These factors may explain how our synthesized AuNPs can simultaneously demonstrate cytotoxicity towards cancer cells via oxidative mechanisms, while also acting as potent antioxidants under different conditions, emphasizing their potential as multifunctional agents in biomedical applications.

5. Conclusions

This study successfully demonstrated the green synthesis of gold nanoparticles using *Scabiosa palaestina* ethanolic extract. As far as we know, this is the first report of AuNPs synthesis from this plant. The biosynthesized AuNPs were spherical, well-dispersed, and exhibited a crystalline face-centered cubic structure. They showed potent anticancer activity against multiple cancer cell lines, particularly 22Rv1 and MDA-MB-231. Moreover, the AuNPs exhibited strong, concentration-dependent antioxidant activity in both the DPPH assay and H_2O_2 assays. These findings highlight the potential of *Scabiosa palaestina*-derived AuNPs for diverse biomedical applications. Future work will aim to optimize the synthesis conditions, including pH and solvent type, to enhance AuNPs stability and reduce particle size. Additionally, further studies will investigate the antimicrobial and antidiabetic activities of these nanoparticles to expand their therapeutic applications.

Author Contributions: Conceptualization, H.H., D.P. and E.B.; methodology, H.H., G.A.B., N.K. and R.E.K.; data curation, H.H., A.B., G.A., N.K., R.E.K., D.P., M.M. and E.B.; writing—original draft preparation, H.H.; writing—review and editing, A.B., D.P., M.M. and E.B.; supervision, D.P.; E.B.; funding acquisition, A.B., M.M. and E.B. All authors have read and agreed to the published version of the manuscript.

Funding: The authors would like to thank the University Research Board (URB) of the American University of Beirut and the University of Petra for their support.

Data Availability Statement: This paper has all the data supporting the findings.

Acknowledgments: The authors acknowledge BioRender for their professional services.

Conflicts of Interest: The authors declare no conflict of interest.

References

1. Venkatraman, G.; Ramya; Shruthilaya; Akila; Ganga; Suresh Kumar; Yoganathan; Santosham, R.; Ponraju. Nanomedicine: Towards Development of Patient-Friendly Drug-Delivery Systems for Oncological Applications. *IJN* **2012**, 1043. https://doi.org/10.2147/IJN.S25182.
2. Botteon, C. E. A.; Silva, L. B.; Ccana-Ccapatinta, G. V.; Silva, T. S.; Ambrosio, S. R.; Veneziani, R. C. S.; Bastos, J. K.; Marcato, P. D. Biosynthesis and Characterization of Gold Nanoparticles Using Brazilian Red Propolis and Evaluation of Its Antimicrobial and Anticancer Activities. *Sci Rep* **2021**, *11* (1), 1974. https://doi.org/10.1038/s41598-021-81281-w.
3. Tahir, K.; Nazir, S.; Li, B.; Khan, A. U.; Khan, Z. U. H.; Gong, P. Y.; Khan, S. U.; Ahmad, A. Nerium Oleander Leaves Extract Mediated Synthesis of Gold Nanoparticles and Its Antioxidant Activity. Materials Letters 2015, 156, 198–201. https://doi.org/10.1016/j.matlet.2015.05.062.
4. Badeggi, U.; Ismail, E.; Adeloye, A.; Botha, S.; Badmus, J.; Marnewick, J.; Cupido, C.; Hussein, A. Green Synthesis of Gold Nanoparticles Capped with Procyanidins from Leucosidea Sericea as Potential Antidiabetic and Antioxidant Agents. Biomolecules 2020, 10 (3), 452. https://doi.org/10.3390/biom10030452.
5. Payne, J.; Badwaik, V.; Waghwani, H. K.; Moolani, H.; Tockstein, S.; Thompson, D.; Dakshinamurthy, R. Development of Dihydrochalcone-Functionalized Gold Nanoparticles for Augmented Antineoplastic Activity. IJN 2018, Volume 13, 1917–1926. https://doi.org/10.2147/IJN.S143506.

 doi:10.20944/preprints202508.0316.v1

6. Huang, X.; El-Sayed, M. A. Gold Nanoparticles: Optical Properties and Implementations in Cancer Diagnosis and Photothermal Therapy. Journal of Advanced Research 2010, 1 (1), 13–28. https://doi.org/10.1016/j.jare.2010.02.002.
7. Fouda, A.; Eid, A. M.; Guibal, E.; Hamza, M. F.; Hassan, S. E.-D.; Alkhalifah, D. H. M.; El-Hossary, D. Green Synthesis of Gold Nanoparticles by Aqueous Extract of Zingiber Officinale: Characterization and Insight into Antimicrobial, Antioxidant, and In Vitro Cytotoxic Activities. Applied Sciences 2022, 12 (24), 12879. https://doi.org/10.3390/app122412879.
8. Duan, H.; Wang, D.; Li, Y. Green Chemistry for Nanoparticle Synthesis. Chem. Soc. Rev. 2015, 44 (16), 5778–5792. https://doi.org/10.1039/C4CS00363B.
9. Amina, S. J.; Guo, B. A Review on the Synthesis and Functionalization of Gold Nanoparticles as a Drug Delivery Vehicle. IJN 2020, Volume 15, 9823–9857. https://doi.org/10.2147/IJN.S279094.
10. Patra, D.; El Kurdi, R. Curcumin as a Novel Reducing and Stabilizing Agent for the Green Synthesis of Metallic Nanoparticles. Green Chemistry Letters and Reviews 2021, 14 (3), 474–487. https://doi.org/10.1080/17518253.2021.1941306.
11. Pinto, D. C. G. A.; Rahmouni, N.; Beghidja, N.; Silva, A. M. S. Scabiosa Genus: A Rich Source of Bioactive Metabolites. Medicines 2018, 5 (4), 110. https://doi.org/10.3390/medicines5040110.
12. Wehbe, N.; Mesmar, J. E.; El Kurdi, R.; Al-Sawalmih, A.; Badran, A.; Patra, D.; Baydoun, E. Halodule Uninervis Extract Facilitates the Green Synthesis of Gold Nanoparticles with Anticancer Activity. Sci Rep 2025, 15 (1), 4286. https://doi.org/10.1038/s41598-024-81875-0.
13. Jyoti, K.; Baunthiyal, M.; Singh, A. Characterization of Silver Nanoparticles Synthesized Using Urtica Dioica Linn. Leaves and Their Synergistic Effects with Antibiotics. Journal of Radiation Research and Applied Sciences 2016, 9 (3), 217–227. https://doi.org/10.1016/j.jrras.2015.10.002.
14. Al Saqr, A.; Khafagy, E.-S.; Alalaiwe, A.; Aldawsari, M. F.; Alshahrani, S. M.; Anwer, Md. K.; Khan, S.; Lila, A. S. A.; Arab, H. H.; Hegazy, W. A. H. Synthesis of Gold Nanoparticles by Using Green Machinery: Characterization and In Vitro Toxicity. Nanomaterials 2021, 11 (3), 808. https://doi.org/10.3390/nano11030808.
15. Rajan, A.; Vilas, V.; Philip, D. Studies on Catalytic, Antioxidant, Antibacterial and Anticancer Activities of Biogenic Gold Nanoparticles. Journal of Molecular Liquids 2015, 212, 331–339. https://doi.org/10.1016/j.molliq.2015.09.013.
16. Department of Botany, University College of Science, Osmania University, Hyderabad, Telangana, -500 007 India; Hymavathi, K.; Sabitha Rani, A.; Department of Botany, University College of Science, Osmania University, Hyderabad, Telangana, -500 007 India. Synthesis and Characterization of Gold Nanoparticles (AuNPs) from Chrozophora Rottleri (Geiseler) Spreng. An Evaluation of Antioxidant and Antimicrobial Activities. AMSR 2024, 3 (2), 1–14. https://doi.org/10.51470/AMSR.2024.03.02.01.
17. Ahmad, T.; Bustam, M. A.; Irfan, M.; Moniruzzaman, M.; Anwaar Asghar, H. M.; Bhattacharjee, S. Green Synthesis of Stabilized Spherical Shaped Gold Nanoparticles Using Novel Aqueous Elaeis Guineensis (Oil Palm) Leaves Extract. Journal of Molecular Structure 2018, 1159, 167–173. https://doi.org/10.1016/j.molstruc.2017.11.095.
18. G., S.; Jha, P. K.; V., V.; C., R.; M., J.; M., S.; Jha, R.; S., S. Cannonball Fruit (Couroupita Guianensis, Aubl.) Extract Mediated Synthesis of Gold Nanoparticles and Evaluation of Its Antioxidant Activity. Journal of Molecular Liquids 2016, 215, 229–236. https://doi.org/10.1016/j.molliq.2015.12.043.
19. Lenzen, S.; Lushchak, V. I.; Scholz, F. The Pro-Radical Hydrogen Peroxide as a Stable Hydroxyl Radical Distributor: Lessons from Pancreatic Beta Cells. Arch Toxicol 2022, 96 (7), 1915–1920. https://doi.org/10.1007/s00204-022-03282-6.
20. Tejero, I.; González-Lafont, À.; Lluch, J. M.; Eriksson, L. A. Theoretical Modeling of Hydroxyl-Radical-Induced Lipid Peroxidation Reactions. J. Phys. Chem. B 2007, 111 (20), 5684–5693. https://doi.org/10.1021/jp0650782.
21. Mahmood, A. S.; Ibrahim, N. M.; Abdul-Jalil, T. Z. Anti- Psoriatic Effect and Phytochemical Evaluation of Iraqi Scabiosa Palaestina Ethyl Acetate Extract. Plant Sci. Today 2024. https://doi.org/10.14719/pst.3055.

 doi:10.20944/preprints202508.0316.v1

22. Khamees, A. H.; Kadhim, E. J. Isolation, Characterization and Quantification of a Pentacyclic Triterpinoid Compound Ursolic Acid in Scabiosa Palaestina L. Distributed in the North of Iraq. Plant Sci. Today 2021. https://doi.org/10.14719/pst.1398.
23. Manivasagan, P.; Venkatesan, J.; Senthilkumar, K.; Sivakumar, K.; Kim, S.-K. Biosynthesis, Antimicrobial and Cytotoxic Effect of Silver Nanoparticles Using a Novel Nocardiopsis Sp. MBRC-1. BioMed Research International 2013, 2013, 1–9. https://doi.org/10.1155/2013/287638.
24. Asker, A. Y. M.; Al Haidar, A. H. M. J. Green Synthesis of Gold Nanoparticles Using Pelargonium Graveolens Leaf Extract: Characterization and Anti-Microbial Properties (An in-Vitro Study). F1000Res 2024, 13, 572. https://doi.org/10.12688/f1000research.150769.2.
25. Ghramh, H. A.; Khan, K. A.; Ibrahim, E. H.; Setzer, W. N. Synthesis of Gold Nanoparticles (AuNPs) Using Ricinus Communis Leaf Ethanol Extract, Their Characterization, and Biological Applications. Nanomaterials 2019, 9 (5), 765. https://doi.org/10.3390/nano9050765.
26. Islam, N. U.; Jalil, K.; Shahid, M.; Muhammad, N.; Rauf, A. Pistacia Integerrima Gall Extract Mediated Green Synthesis of Gold Nanoparticles and Their Biological Activities. Arabian Journal of Chemistry 2019, 12 (8), 2310–2319. https://doi.org/10.1016/j.arabjc.2015.02.014.
27. Long, N. N.; Vu, L. V.; Kiem, C. D.; Doanh, S. C.; Nguyet, C. T.; Hang, P. T.; Thien, N. D.; Quynh, L. M. Synthesis and Optical Properties of Colloidal Gold Nanoparticles. J. Phys.: Conf. Ser. 2009, 187, 012026. https://doi.org/10.1088/1742-6596/187/1/012026.
28. Fathi, F.; Rashidi, M.-R.; Omidi, Y. Ultra-Sensitive Detection by Metal Nanoparticles-Mediated Enhanced SPR Biosensors. Talanta 2019, 192, 118–127. https://doi.org/10.1016/j.talanta.2018.09.023.
29. Ozgur, M. U.; Ortadoğulu, E.; ErdemiR, B. Greener Approach to Synthesis of Steady Nano-Sized Gold with the Aqueous Concentrate of Cotinus Coggygria Scop. Leaves. Gazi University Journal of Science 2021, 34 (2), 406–421. https://doi.org/10.35378/gujs.752304.
30. Hutchinson, N.; Wu, Y.; Wang, Y.; Kanungo, M.; DeBruine, A.; Kroll, E.; Gilmore, D.; Eckrose, Z.; Gaston, S.; Matel, P.; Kaltchev, M.; Nickel, A.-M.; Kumpaty, S.; Hua, X.; Zhang, W. Green Synthesis of Gold Nanoparticles Using Upland Cress and Their Biochemical Characterization and Assessment. Nanomaterials 2021, 12 (1), 28. https://doi.org/10.3390/nano12010028.
31. Maliszewska, I.; Wanarska, E.; Thompson, A. C.; Samuel, I. D. W.; Matczyszyn, K. Biogenic Gold Nanoparticles Decrease Methylene Blue Photobleaching and Enhance Antimicrobial Photodynamic Therapy. Molecules 2021, 26 (3), 623. https://doi.org/10.3390/molecules26030623.
32. Hatipoğlu, A. Rapid Green Synthesis of Gold Nanoparticles: Synthesis, Characterization, and Antimicrobial Activities. https://doi.org/10.23751/pn.v23i3.11988
33. Stalin Dhas, T.; Ganesh Kumar, V.; Stanley Abraham, L.; Karthick, V.; Govindaraju, K. Sargassum Myriocystum Mediated Biosynthesis of Gold Nanoparticles. Spectrochimica Acta Part A: Molecular and Biomolecular Spectroscopy 2012, 99, 97–101. https://doi.org/10.1016/j.saa.2012.09.024.
34. Arockiya Aarthi Rajathi, F.; Parthiban, C.; Ganesh Kumar, V.; Anantharaman, P. Biosynthesis of Antibacterial Gold Nanoparticles Using Brown Alga, Stoechospermum Marginatum (Kützing). Spectrochimica Acta Part A: Molecular and Biomolecular Spectroscopy 2012, 99, 166–173. https://doi.org/10.1016/j.saa.2012.08.081.
35. Kalantari, H.; Turner, R. J. Structural and Antimicrobial Properties of Synthesized Gold Nanoparticles Using Biological and Chemical Approaches. Front. Chem. 2024, 12, 1482102. https://doi.org/10.3389/fchem.2024.1482102.
36. Dhas, T. S.; Kumar, V. G.; Karthick, V.; Govindaraju, K.; Shankara Narayana, T. Biosynthesis of Gold Nanoparticles Using Sargassum Swartzii and Its Cytotoxicity Effect on HeLa Cells. Spectrochimica Acta Part A: Molecular and Biomolecular Spectroscopy 2014, 133, 102–106. https://doi.org/10.1016/j.saa.2014.05.042.
37. Danaei, M.; Dehghankhold, M.; Ataei, S.; Hasanzadeh Davarani, F.; Javanmard, R.; Dokhani, A.; Khorasani, S.; Mozafari, M. R. Impact of Particle Size and Polydispersity Index on the Clinical Applications of Lipidic Nanocarrier Systems. Pharmaceutics 2018, 10 (2), 57. https://doi.org/10.3390/pharmaceutics10020057.
38. Bhattacharjee, S. DLS and Zeta Potential – What They Are and What They Are Not? Journal of Controlled Release 2016, 235, 337–351. https://doi.org/10.1016/j.jconrel.2016.06.017.

 doi:10.20944/preprints202508.0316.v1

39. Xin Lee, K.; Shameli, K.; Miyake, M.; Kuwano, N.; Bt Ahmad Khairudin, N. B.; Bt Mohamad, S. E.; Yew, Y. P. Green Synthesis of Gold Nanoparticles Using Aqueous Extract of Garcinia Mangostana Fruit Peels. Journal of Nanomaterials 2016, 2016, 1–7. https://doi.org/10.1155/2016/8489094.
40. Koliyote, S.; Shaji, J. A Recent Review on Synthesis, Characterization and Activities of Gold Nanoparticles Using Plant Extracts. Ind. J. Pharm. Edu. Res 2023, 57 (2s), s198–s212. https://doi.org/10.5530/ijper.57.2s.24.
41. Talebi Tadi, A.; Farhadiannezhad, M.; Nezamtaheri, M. S.; Goliaei, B.; Nowrouzi, A. Biosynthesis and Characterization of Gold Nanoparticles from Citrullus Colocynthis (L.) Schrad Pulp Ethanolic Extract: Their Cytotoxic, Genotoxic, Apoptotic, and Antioxidant Activities. Heliyon 2024, 10 (16), e35825. https://doi.org/10.1016/j.heliyon.2024.e35825.
42. Soto, K. M.; López-Romero, J. M.; Mendoza, S.; Peza-Ledesma, C.; Rivera-Muñoz, E. M.; Velazquez-Castillo, R. R.; Pineda-Piñón, J.; Méndez-Lozano, N.; Manzano-Ramírez, A. Rapid and Facile Synthesis of Gold Nanoparticles with Two Mexican Medicinal Plants and a Comparison with Traditional Chemical Synthesis. Materials Chemistry and Physics 2023, 295, 127109. https://doi.org/10.1016/j.matchemphys.2022.127109.
43. Steckiewicz, K. P.; Barcinska, E.; Malankowska, A.; Zauszkiewicz–Pawlak, A.; Nowaczyk, G.; Zaleska-Medynska, A.; Inkielewicz-Stepniak, I. Impact of Gold Nanoparticles Shape on Their Cytotoxicity against Human Osteoblast and Osteosarcoma in in Vitro Model. Evaluation of the Safety of Use and Anti-Cancer Potential. J Mater Sci: Mater Med 2019, 30 (2), 22. https://doi.org/10.1007/s10856-019-6221-2.
44. Jannathul Firdhouse, M.; Lalitha, P. Cytotoxicity of Spherical Gold Nanoparticles Synthesised Using Aqueous Extracts of Aerial Roots of Rhaphidophora Aurea (Linden Ex Andre) Intertwined over Lawsonia Inermis and Areca Catechu on MCF-7 Cell Line. IET nanobiotechnol. 2017, 11 (1), 2–11. https://doi.org/10.1049/iet-nbt.2016.0076.
45. Assad, N.; Laila, M. B.; Hassan, M. N. U.; Rehman, M. F. U.; Ali, L.; Mustaqeem, M.; Ullah, B.; Khan, M. N.; Iqbal, M.; Ercişli, S.; Alarfaj, A. A.; Ansari, M. J.; Malik, T. Eco-Friendly Synthesis of Gold Nanoparticles Using Equisetum Diffusum D. Don. with Broad-Spectrum Antibacterial, Anticancer, Antidiabetic, and Antioxidant Potentials. Sci Rep 2025, 15 (1), 19246. https://doi.org/10.1038/s41598-025-02450-9.
46. Oueslati, M. H.; Tahar, L. B.; Harrath, A. H. Catalytic, Antioxidant and Anticancer Activities of Gold Nanoparticles Synthesized by Kaempferol Glucoside from Lotus Leguminosae. Arabian Journal of Chemistry 2020, 13 (1), 3112–3122. https://doi.org/10.1016/j.arabjc.2018.09.003.
47. Rajeshkumar, S.; Parameswari, R. P.; Jayapriya, J.; Tharani, M.; Ali, H.; Aljarba, N. H.; Alkahtani, S.; Alarifi, S. [Retracted] Apoptotic and Antioxidant Activity of Gold Nanoparticles Synthesized Using Marine Brown Seaweed: An In Vitro Study. *BioMed Research International* **2022**, *2022* (1), 5746761. https://doi.org/10.1155/2022/5746761.
48. Sowmya, K.; Narendhirakannan, R. Green Synthesis, Characterization and Bioactivity of AuNPs from E. Cardamomum: A Comparative Study. Int J. Pharm. Investigation 2025, 15 (2), 417–433. https://doi.org/10.5530/ijpi.20250039.
49. Suliasih, B. A.; Budi, S.; Katas, H. Synthesis and Application of Gold Nanoparticles as Antioxidants. PHAR 2024, 71, 1–19. https://doi.org/10.3897/pharmacia.71.e112322.
50. Kim, S.; Ryu, D. Silver Nanoparticle-induced Oxidative Stress, Genotoxicity and Apoptosis in Cultured Cells and Animal Tissues. J of Applied Toxicology 2013, 33 (2), 78–89. https://doi.org/10.1002/jat.2792.
51. Manke, A.; Wang, L.; Rojanasakul, Y. Mechanisms of Nanoparticle-Induced Oxidative Stress and Toxicity. BioMed Research International 2013, 2013, 1–15. https://doi.org/10.1155/2013/942916.